Journal of Thermal Analysis and Calorimetry, Vol. 88 (2007) 1, 225–230

REACTIVITY OF A Ti–45.9Al–8Nb ALLOY IN AIR AT 700–900°C

Elżbieta Godlewska[1*], *M. Mitoraj*[1], *F. Devred*[2] *and B. E. Nieuwenhuys*[2]

[1]Faculty of Material Science and Ceramics, AGH-UST, Krakow, Poland
[2]University of Leiden, The Netherlands

A Ti–45.9Al–8Nb (at%) alloy with a lamellar structure ($\gamma+\alpha_2$) was oxidised in air at 700, 800, 850 and 900°C in isothermal and thermal cycling conditions. The reaction progress was followed by thermogravimetric measurements. In isothermal conditions the oxidation kinetics followed approximately a parabolic rate law and the rate constants ranged from about 10^{-12} kg^2 m^{-4} s^{-1} at 700°C to 10^{-10} kg^2 m^{-4} s^{-1} at 900°C. The oxide scales were built of Al_2O_3 and TiO_2, the former being the main component of the outermost layer. The oxidation behaviour of Ti–45.9Al–8Nb was referred to a commercial titanium alloy, WT4 (Ti–6Al–1Mn), and selected oxidation-resistant alloys.

Keywords: *oxidation kinetics, oxide scale structure and composition, γ-TiAl*

Introduction

Titanium aluminides are perceived as attractive structural materials because of their low density (3.7–3.9 g cm^{-3}) and good mechanical properties at elevated temperatures (tensile strength and creep strength) [1–4]. Among the intermetallic compounds based on titanium and aluminium, only Ti_3Al (α_2) with a hexagonal structure and TiAl (γ) with a tetragonal structure are extensively studied [5, 6]. The envisaged applications of titanium aluminide alloys include compressor blades [7, 8]. Replacing the conventional nickel-base or iron-base superalloys by novel TiAl alloys might result in a 50% reduction of the components mass. However, the use of these alloys is hindered by a too low ductility at room temperature and still inadequate oxidation resistance at temperatures higher than 800°C [9, 10]. The oxidation products of TiAl alloys are both rutile (TiO_2) and corundum (Al_2O_3) because of similar activities of titanium and aluminium in the alloy and similar affinity of both metals for oxygen. Titania unlike alumina has high oxygen diffusivity and poor protective properties [11, 12]. Some earlier studies indicate that approximately 60–70% of aluminium is needed for a binary Ti–Al alloy to form a continuous Al_2O_3 scale in air [13, 14].

There are two major ways to increase the oxidation resistance of TiAl, i.e. alloying and surface modification. A number of ternary [15–18] and quaternary [19, 20] additions are described in the literature. Among those, an especially interesting one is niobium [21–24]. The effect of niobium on the oxidation behaviour of titanium aluminides is complex and not yet fully understood. It is suggested that Nb replaces Ti ions in TiO_2, thus reducing the concentration of anion vacancies and the diffusivity of oxygen. Another possible effect is that niobium favours the formation of alumina scale by increasing the thermodynamic activity of aluminium relative to titanium. Niobium is also known to improve mechanical properties of the TiAl alloys, such as ductility and room-temperature toughness [25].

Many different methods of improving the oxidation resistance of TiAl alloys by surface modification are reported in the literature. Especially interesting ones are the following: pack cementation [26–29], magnetron sputtering [30–33] and ion implantation [34–37].

The purpose of this work was to assess the reactivity of Ti–45.9Al–8Nb alloy in air in the temperature range 700–900°C.

Experimental

The Ti–45.9Al–8Nb ingots, produced by horizontal centrifugal casting and HIP-ing, were cut into disks, 16 mm in diameter and 0.8–1.0 mm in thickness, ground with emery papers up to 1200 grit number, and finally washed with distilled water and acetone. The reference specimens of Ti–6Al–1Mn, in a form of half-discs, 17 mm in diameter and 1.0–1.5 mm in thickness, were given a similar surface finish.

The isothermal oxidation tests were carried out at 700, 800 and 900°C in laboratory air with average humidity of 35%. The mass changes were continuously recorded by means of a thermobalance (MK2 Vacuum Head CI Electronics Ltd.) with an accuracy of 10^{-6} g.

The cyclic oxidation tests were conducted in the temperature range 700–850°C. Long (20-h) and short (1-h) cycles were used. Each cycle comprised rapid

* Author for correspondence: godlewsk@agh.edu.pl

1388–6150/$20.00

Akadémiai Kiadó, Budapest, Hungary
Springer, Dordrecht, The Netherlands

heating to the test temperature, maintaining at the temperature for 1 or 20 h and rapid cooling to the room temperature. In the long-cycle tests, the mass changes were measured after every cycle. In the short-cycle tests, the mass changes were measured once a day. The accuracy of mass change measurements was 10^{-4} g. During the cyclic oxidation tests, the specimens were kept in alumina crucibles in order to collect oxides lost by spallation.

After oxidation the scales were examined by means of optical microscopy (OM) and scanning electron microscopy (Nova Nano SEM 200). Phase and chemical compositions of the oxidation products were analysed by X-ray diffraction (Seifert XRD7), energy dispersive X-ray spectroscopy (EDS) and X-ray photoelectron spectroscopy (XPS). Cross-sections of the selected samples were examined by SEM using secondary electron images and backscattered electron images (SEI and BEI) as well as by transmission electron microscopy (TEM-PHILIPS CM 20–200 kV TWIN).

Results and discussion

Isothermal oxidation kinetics

The isothermal kinetic curves at 700, 800 and 900°C are presented in Fig. 1. The parabolic plot was used because it was expected that the scale growth on the Ti–45.9Al–8Nb alloy would be controlled by diffusion. Actually, oxidation of the Ti–45.9Al–8Nb alloy followed approximately a parabolic rate law after some initial period, where relatively high mass gains were recorded. The early stages probably involved adsorption and diffusion of gases, as well as nucleation and growth of oxide grains on alloy surface. In order to compare the oxidation kinetics of the investigated material with some scaling resistant alloys, the parabolic rate constants of oxidation were calculated. The lowest rate constant, at the 700°C, was about $(3.71\pm0.07)\cdot10^{-13}$ kg^2 m^{-4} s^{-1}, at 800 and 900°C the rate constants were higher and amounted to $(1.981\pm0.002)\cdot10^{-11}$ and $(3.28\pm0.02)\cdot10^{-11}$ kg^2 m^{-4} s^{-1}, respectively.

Figure 2 shows the parabolic rate constants (k_p) of the Ti–45.9Al–8Nb alloy in comparison with some alumina formers, such as NiAl, FeAl and Ni-base superalloy. As can be seen, at 700°C, the value of kp calculated for the Ti–45.9Al–8Nb alloy is close to the growth rates of Al_2O_3 on highly oxidation-resistant materials at 900°C.

The activation energy of the Ti–45.9Al–8Nb alloy oxidation was about 200 kJ mol^{-1}, i.e. comparable with that of pure titanium oxidation (180–230 kJ mol^{-1}).

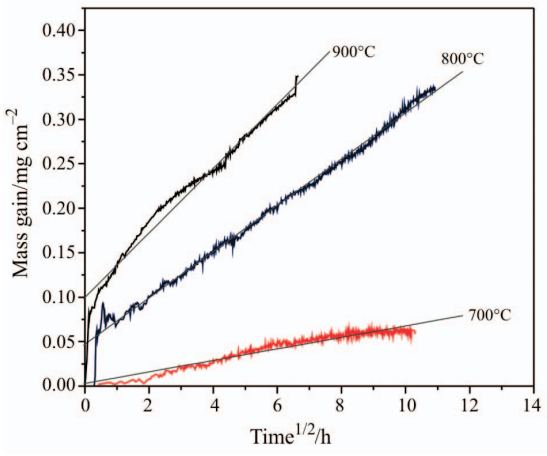

Fig. 1 Oxidation kinetics of the Ti–45.9Al–8Nb alloy in air at 700, 800 and 900°C in a parabolic plot

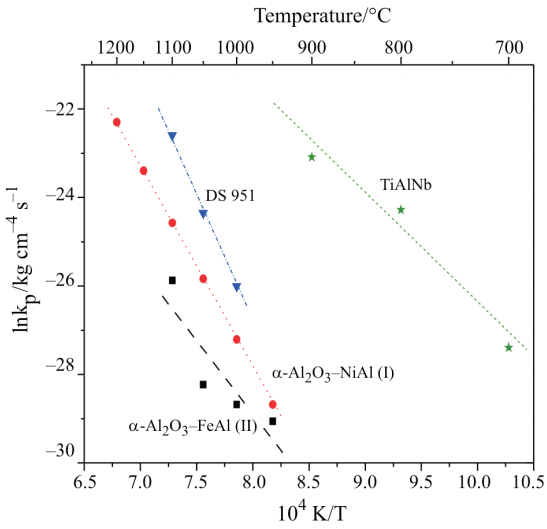

Fig. 2 Temperature dependence of the parabolic rate constant of oxidation for the Ti–45.9Al–8Nb alloy and several highly oxidation resistant materials: [38] – NiAl, [39] – FeAl and [40] – Ni-base superalloy DS951

Cyclic oxidation kinetics

Thermal cycling oxidation tests were used to simulate real corrosion environments. These tests allow the assessment of scale adherence and its susceptibility to cracking or spallation under the influence of thermal stresses.

Mass changes of the Ti–45.9Al–8Nb specimens during 1-h cycle tests at four different temperatures are shown in Fig. 3. In general, the specimen mass increased with time and temperature of oxidation. The slight mass losses, visible on the plot, were not related with scale decoherence but probably with handling of the specimens – no spalled oxides were collected in alumina crucibles.

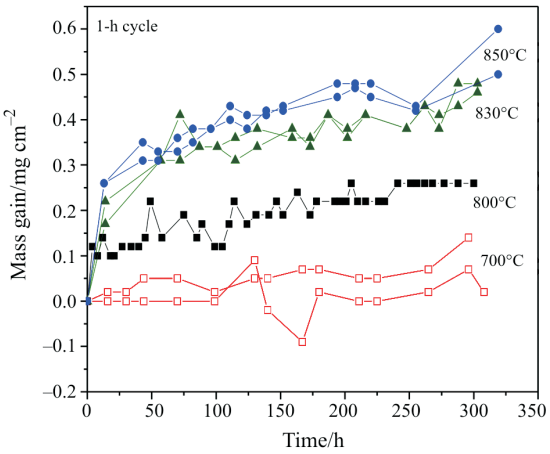

Fig. 3 Mass changes of the Ti–45.9Al–8Nb alloy in cyclic oxidation tests at four different temperatures: 700, 800, 830 and 850°C (1-h cycles)

In Fig. 4 mass variations of the Ti–45.9Al–8Nb and the Ti–6Al–1Mn alloys are compared during oxidation at 700°C. The Ti–45.9Al–8Nb alloy maintained excellent oxidation resistance for at least 1000 h. After 300 h the measured mass change of Ti–6Al–1Mn (4.3 mg cm^{-2}) was about 40 times higher than that of Ti–45.9Al–8Nb (0.10 mg cm^{-2}). The differences visibly increased at 800°C (Fig. 5). After 240 h of oxidation, Ti–6Al–1Mn showed a 60 times higher mass gain relative to Ti–45.9Al–8Nb and intensive scale spallation (Fig. 6).

Scale morphology

Figure 7 presents SEM micrographs of the specimen surface and cross-section after 20, 80 and 340 h of oxidation in air (20-h cycle). The scale is built of small equiaxed grains (Fig. 7a), which get coarser with time. There is no evidence of scale cracking or

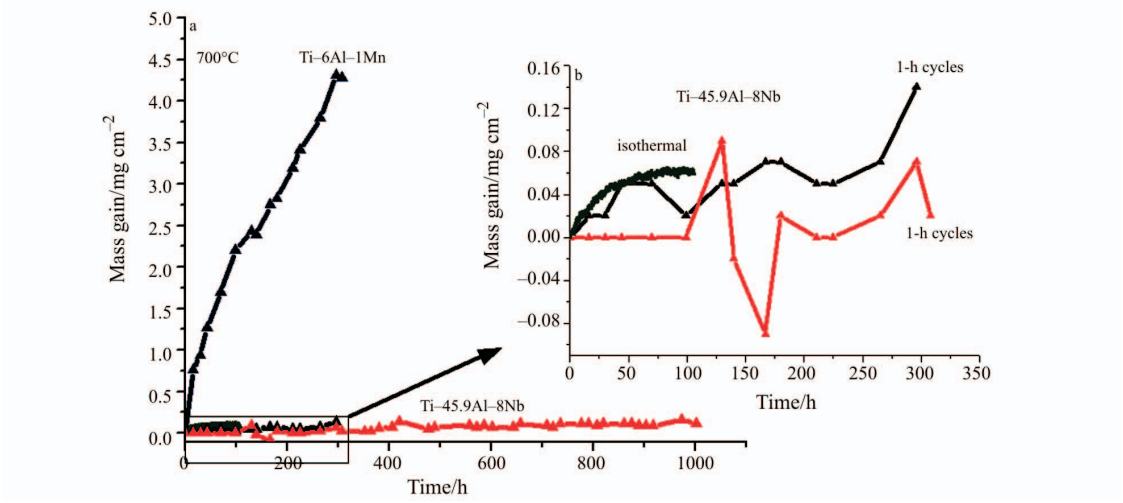

Fig. 4 a – Mass changes of Ti–45.9Al–8Nb during oxidation in air at 700°C (1-h cycles and isothermal conditions) compared with gross mass changes of Ti–6Al–1Mn (1-h cycles); b – area of graph (a) at a higher magnification

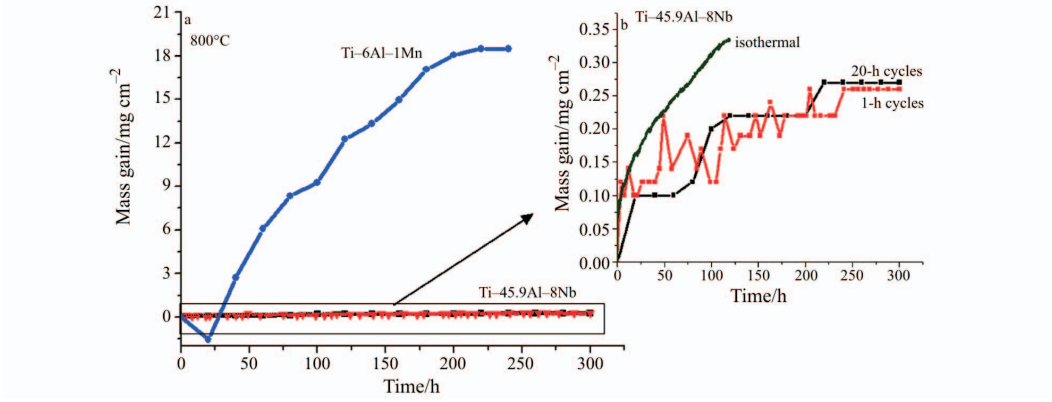

Fig. 5 a – Mass changes of the Ti–45.9Al–8Nb alloy during oxidation in air at 800°C (1-h cycles, 20-h cycles and isothermal conditions) compared with gross mass changes of the Ti–6Al–1Mn alloy (20-h cycles); b – area of graph (a) at a higher magnification

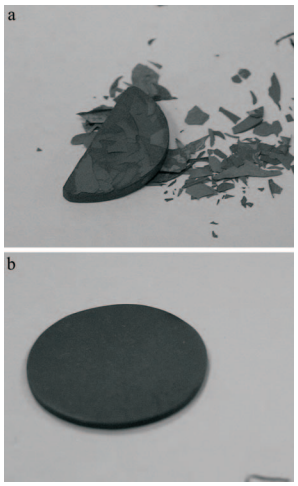

Fig. 6 Samples of a – Ti–6Al–1Mn and b – Ti–45.9Al–8Nb after 240 h of cyclic oxidation (20-h cycles) in air at 800°C

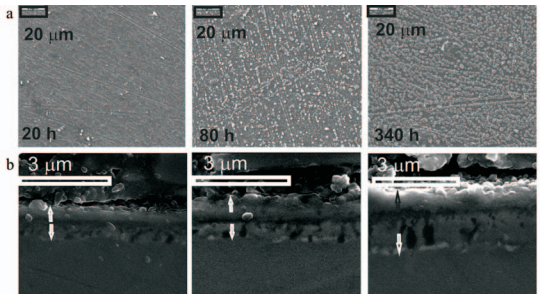

Fig. 7 SEM micrographs of a – scale surfaces and b – cross-sections after 20, 80 and 340 h of cyclic oxidation of the Ti–45.9Al–8Nb alloy in air at 800°C (20-h cycles)

spallation. As can be seen in Fig. 7b, scale thickness increases with oxidation time.

Figure 8 shows SEM micrographs of the scale surfaces after 120 h of isothermal oxidation at 700, 800 and 900°C. Differences in grain size and shape are clearly visible. As follows from Figs 7 and 8, the grain size of the scale increased with time and temperature of oxidation.

Excellent scale adherence is evidenced in Fig. 9, presenting a micrograph of a fractured specimen after the oxidation test at 850°C. A lamellar structure of the Ti–45.9Al–8Nb alloy is also revealed.

Composition of the scale

Chemical composition of the scale was analysed by several methods. In Fig. 10A, the X-ray element maps from a cross-section of the Ti–45.9Al–8Nb sample oxidised in air for 140 h at 850°C show that aluminium as well as oxygen are the main elements present on the scale surface. The X-ray element distribution (Fig. 10B_b) along the line marked in Fig. 10B_a confirms the presence of aluminium and oxygen in the outermost layer of the scale. This may indicate

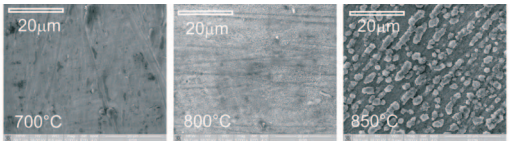

Fig. 8 SEM micrographs of scale surface after 120 h of isothermal oxidation of the Ti–45.9Al–8Nb alloy at 700, 800 and 900°C

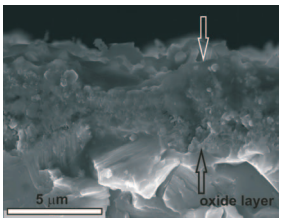

Fig. 9 SEM micrograph of the fractured Ti–45.9Al–8Nb specimen oxidised in air at 850°C for 120 h

that Al and O are components of one phase, i.e. aluminium oxide (Al_2O_3).

The XPS analysis was performed with an ESCALAB MKII (VG scientific) system equipped with a dual anode X-ray source (Mg/Al) and a spherical analyzer. The instrument was set at a constant analyzer pass energy of 50 eV and Al–$K_{\alpha_{1,2}}$ radiation with a photon energy of 1486.6 eV was used for excitation. Spectra were recorded of the Ti 2p, Al 2s, Al 2p, O 1s and C 1s photoelectron lines with a step size of 0.1 eV. The spectra shown in Fig. 11 were corrected for satellites caused by the non-monochromatic nature of the incident X-ray source. The carbon C 1s peak (285 eV) was used as internal reference in order to correct for the shift in binding energy due to charging of the sample. The surface composition in Fig. 11 was determined from the integrated intensity of the Ti 2p, Al 2p photoelectron lines by adopting the elemental sensitivity factors [41, 42]. The CasaXPS software was used to deconvolute the recorded spectra. The accuracy of ±2 at% was defined by repeating both measurement and curve fitting. According to the XPS analysis (Fig. 11), aluminium oxide Al_2O_3 is probably formed at the early stages of oxidation. In the oxidised sample, only TiO_2 is present: the Ti 2p3/2 peak at 458 eV with a doublet separation around 5.5 eV, is characteristic of TiO_2. In the non-oxidised sample, TiO_2 is still the main Ti compound present at the surface, but, clearly, another peak is also present at lower binding energy. It is difficult to discriminate between TiO, Ti_2O_3 and metallic Ti that all have binding energies around 453–454 eV in the Ti 2p3/2 area. The doublet separation (6.1 eV for metallic Ti, 5.5 eV for Ti oxides) should permit to identify the peak but the overlap with TiO_2 peak makes it difficult. Only aluminium oxide is present in the oxidised sample (Al_2O_3 at 74 eV). In the non-oxi-

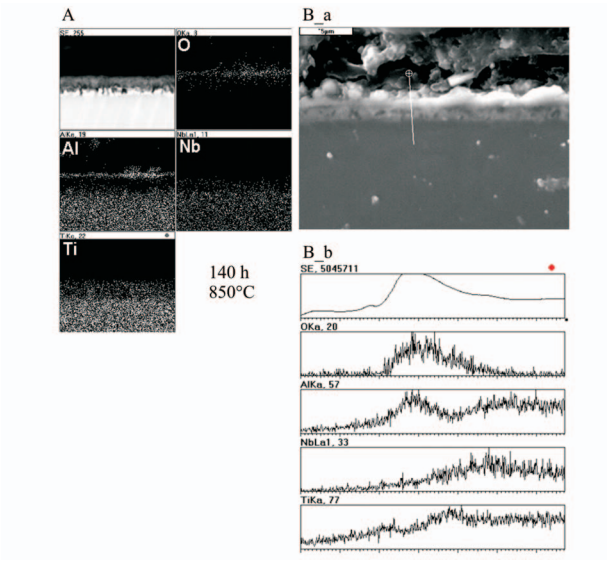

Fig. 10 A – BEI and X-ray element maps from the cross-section of the Ti–45.9Al–8Nb sample after 140 h of isothermal oxidation in air at 850°C; B_a – SEM micrograph of scale cross-section after 300 h of cyclic oxidation in air at 800°C; B_b – X-ray element distribution along the line marked in B_a

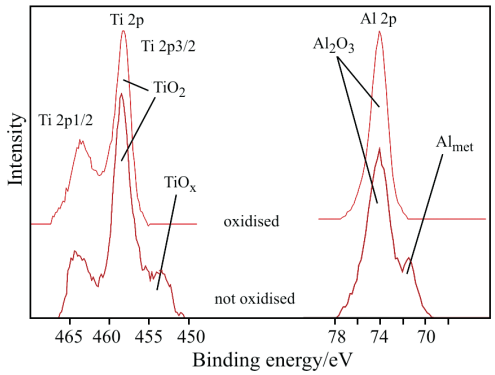

Fig. 11 XPS analysis of Ti–45.9Al–8Nb samples: oxidised for 85 min in air at 800°C and non-oxidised

	Titanium/ at%		Aluminium/ at%		Niobium/ at%
	TiO_2	other	Al_2O_3	metal	oxide
Non-oxidised	20±2	2±2	68±2	10±2	none
Oxidised	5±2	–	95±2	–	traces

dised sample, metallic aluminium is also observed (71 eV). This metallic aluminium contribution might be attributed to aluminium from the alloy underneath, the outer oxide layer being rather thin without any oxidation treatment. Quantitatively, after oxidation, the main phase present in the near surface area is Al_2O_3. The ratio of aluminium oxide to titanium oxide on the surface after 85 min oxidation is 95:5 and it remains almost constant (around 90:10) after an oxidation

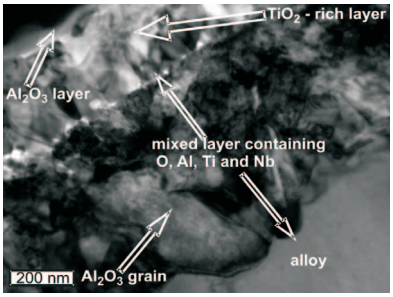

Fig. 12 TEM image of the scale formed on the Ti–45.9Al–8Nb alloy after 300 h of cyclic oxidation in air at 800°C (20-h cycles)

time of about 40 h, independently of the test type (isothermal or cyclic oxidation).

The X-ray diffraction pattern of the oxide scale formed on Ti–45.9Al–8Nb during 300 h of cyclic oxidation in air at 800°C (20-h cycles) shows peaks related mainly to rutile (TiO_2) and corundum (Al_2O_3) and traces of TiN and Ti_3O.

Beneath the Al_2O_3/TiO_2 layer, there is a mixed inner layer containing all alloy components and oxygen (Fig. 12). Near the alloy/scale interface, there are niobium-rich precipitates (bright spots in BEI Fig. 10A and dark spots in TEM image – Fig. 12).

The TEM image (Fig. 12) shows that the alloy/scale interface is slightly undulated, which probably indicates stress generation in the system during thermal cycling (alloy/scale CTE mismatch).

The structure of the oxide scale formed on the Ti–45.9Al–8Nb alloy is complex. According to the investigations carried out so far, it can be stated that aluminium oxide appears on the alloy surface at the early stages of oxidation. The aluminium depleted zone of the alloy underneath oxidises to titanium dioxide doped with niobium. One of possible scenarios of scale evolution is that titanium dioxide, which is not stable in contact with the alloy, decomposes, giving rise to the inner scale layer with non-uniform composition. This hypothesis requires, however, further studies.

Conclusions

- Oxidation of the Ti–45.9Al–8Nb alloy, after some initial period, followed approximately a parabolic rate law. The initial stages of the reaction probably involved adsorption and diffusion of gases, as well as nucleation and growth of oxide grains.
- The parabolic rate constant of oxidation calculated for the Ti–45.9Al–8Nb alloy at 700°C was comparable with the growth rate of Al_2O_3 at 900°C on alumina formers (NiAl, FeAl, Ni-based superalloy).
- The two–phase ($\gamma+\alpha_2$) Ti–45.9Al–8Nb alloy had much better oxidation resistance than the near-α Ti–6Al–1Mn alloy.

- At 700°C the Ti–45.9Al–8Nb alloy showed very good cyclic-oxidation resistance for at least 1000 cycles (1-h cycles).
- Despite some mass fluctuations in cyclic oxidation tests, the scale surfaces were uniform without the symptoms of cracking and spallation. Thin and adherent oxide scales formed on the Ti–45.9Al–8Nb alloy were composed of three main layers: the outermost very thin layer of Al_2O_3, the subjacent layer of TiO_2 doped with niobium and the mixed inner layer containing all alloy components and oxygen.
- Niobium-rich precipitates as well as aluminium oxide precipitates embedded in a titanium-rich matrix were present near the alloy/scale interface.
- The alloy/scale interface was sound and slightly undulated. Deformation of the alloy was probably related to stresses generated in the system upon scale growth and thermal cycling.
- The positive influence of niobium on the oxidation behaviour of TiAl alloys might be related to the modification of their mechanical and thermal properties as well as of the defect structure and transport properties in the alloy/scale system.
- Further studies are necessary to clarify the oxidation mechanism of the ternary Ti–45.9Al–8Nb.

Acknowledgements

The investigations presented in this paper were carried out in the framework of an Integrated Project IMPRESS FP6 EU (Contract No.: 500635). The authors acknowledge financial support from the State Committee for Scientific Research in Poland (Grant No.: 22.22.160.293). TEM/EDS analyses were performed by Dr. Jerzy Morgiel from the Institute of Metallurgy and Materials Science, Polish Academy of Sciences. Ingots of alloy Ti–45.9Al–8Nb were delivered by ACCESS e.V. (Aachen, Germany).

References

1 E. A. Loria, Intermetallics, 8 (2000) 1339.
2 X. Wu, Intermetallics, 14 (2006) 1114.
3 M. Badami and F. Marino, Int. J. Fatigue, 28 (2006) 722.
4 W. E. Voicea, M. Henderson, E. F. J. Shelton and X. Wu, Intermetallics, 13 (2005) 959.
5 S. Djanarthany, J. C. Viala and J. Bouix, Mater. Chem. Phys., 72 (2001) 301.
6 M. Yamaguchi, H. Inui and K. Ito, Acta Mater., 48 (2000) 307.
7 D. M. Dimiduk, Mater. Sci. Eng. A, 263 (1999) 281.
8 E. O. Ezugwu, J. Bonney and Y. Yamamne, J. Mater. Process. Technol., 134 (2003) 233.
9 M. Groß, V. Kolarik and A. Rahmel, Oxid. Met., 48 (1997) 171.
10 M. Schmitz-Niederau and M. Schütze, Oxid. Met., 52 (1999) 225.
11 G. Lütjering and J. C. Williams, Titanium, Springer-Verlag, Berlin Heidelberg, New York 2003, p 48.
12 S. A. Kekare and P. B. Aswath, J. Mater. Sci., 32 (1997) 2845.
13 A. Rahmel, W. J. Quadakkers and M. Shütze, Mater. Corros., 46 (1995) 271.
14 Y. Shida and H. Anada, Mater. Trans. JIM, 34 (1993) 236.
15 H. G. Jung and K. Y. Kim, Oxid. Met., 58 (2002) 197.
16 G. S. Fox-Rabinovich, G. C. Weatherly, D. S. Wilkinson, A. I. Kovalev and D. L. Wainstein, Intermetallics, 12 (2004) 165.
17 Y. Wu, K. Hagihara and Y. Umakoshi, Intermetallics, 12 (2004) 519.
18 Y. Wu, Y. Umakoshi, X. W. Li and T. Narita, Oxid. Met., 66 (2006) 321.
19 D. B. Lee and S. W. Woo, Intermetallics, 13 (2005) 169.
20 C. T. Yang and C. H. Koo, Intermetallics, 12 (2004) 235.
21 X. Ding, Y. Tan, Y. Shen, F. Wang and J.-M. Yang, Key Eng. Mater., 297–300 (2005) 403.
22 H. Jiang, T. S. Rong, D. Hu, I. P. Jones and W. Voice, Intermetallics, 14 (2006) 1433.
23 S. K. Varma, A. Chan and R. N. Mahapatra, Oxid. Met., 55 (2001) 423.
24 H. Jiang, M. Hirohashi, Y. Lu and H. Imanari, Scripta Mater., 46 (2002) 639.
25 Z. C. Liu, J. P. Lin, S. J. Li and G. L. Chen, Intermetallics, 10 (2002) 653.
26 Ch. Zhou, H. Xu, S. Gong and K. Y. Kim, Mater. Sci. Eng. A, 341 (2003) 169.
27 W. Liang, X. X. Ma, X. G. Zhao, F. Zhang, J. Y. Shi and J. Zhang, Intermetallics, 15 (2007) 1.
28 Z. D. Xiang, S. P. Rose and P. K. Datta, Mater. Chem. Phys., 80 (2003) 482.
29 T. Izumi, T. Nishimoto and T. Narita, Intermetallics, 11 (2003) 841.
30 C. Zhou, Y. Yang, S. Gong and H. Xu, Mat. Sci. Eng. A, 307 (2001) 182.
31 Z. Liu and G. Wang, Mater. Sci. Eng. A, 397 (2005) 50.
32 M. S. Chu and S. K. Wu, Acta Mater., 51 (2001) 3109.
33 M. S. Chu and S. K. Wu, Oxid. Met., 63 (2005) 1.
34 H. E. Zschau, M. Schütze, H. Baumann and K. Bethge, Mater. Sci. Forum, 461–464 (2004) 502.
35 H. E. Zschau, M. Schütze, H. Baumann and K. Bethge, Intermetallics, 14 (2006) 1136.
36 X. Y. Li and S. Taniguchi, Mater. Sci. Eng. A, 398 (2005) 268.
37 A. Donchev, E. Richter, M. Schütze and R. Yankov, Intermetallics, 14 (2006) 1168.
38 M. W. Brumm and H. J. Grabke, Corros. Sci., 33 (1992) 1677.
39 I. Rommerskirchen, B. Eltester and H. J. Grabke, Mater. Corros., 47 (1996) 646.
40 L. Huang, X. F. Sun, H. R. Guan and Z. Q. Hu, Oxid. Met., 64 (2005) 303.
41 J. F. Moulder, W. F. Stickle, P. E. Sobol and K. D. Bomben, Handbook of X-ray Photoelectron Spectroscopy, Perkin-Elmer, Wellesley 1992, ISBN 0-962-70262-5.
42 ASTM E902-88, Surf. Interface Anal., 17 (1991) 4709.

DOI: 10.1007/s10973-006-8291-x